

Isolation of Key Organometallic Aryl-Co(III) Intermediates in Cobalt-Catalyzed C(sp²)-H Functionalizations and New Insights into Alkyne Annulation Reaction Mechanisms

Oriol Planas,[†] Christopher J. Whiteoak,^{†,‡} Vlad Martin-Diaconescu,[†] Ilaria Gamba,[†] Josep M. Luis,[†] Teodor Parella,[§] Anna Company,[†] and Xavi Ribas^{*,†}

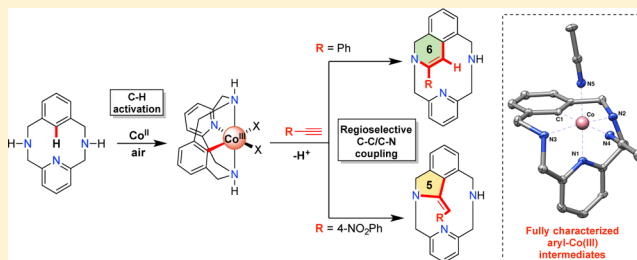
[†]Institut de Química Computacional i Catàlisi (IQCC) and Departament de Química, Universitat de Girona, Campus Montilivi, Girona, E-17071 Catalonia, Spain

[‡]Biomolecular Sciences Research Centre, Faculty of Health and Wellbeing, Sheffield Hallam University, City Campus, Sheffield S1 1WB, England

[§]Servei de RMN, Facultat de Ciències, Universitat Autònoma de Barcelona, Campus UAB, Bellaterra, E-08193 Catalonia, Spain

Supporting Information

ABSTRACT: The selective annulation reaction of alkynes with substrates containing inert C–H bonds using cobalt as catalyst is currently a topic attracting significant interest. Unfortunately, the mechanism of this transformation is still relatively poorly understood, with little experimental evidence for intermediates, although an organometallic Co(III) species is generally implicated. Herein, we describe a rare example of the preparation and characterization of benchtop-stable organometallic aryl-Co(III) compounds (NMR, HRMS, XAS, and XRD) prepared through a C(sp²)-H activation, using a model macrocyclic arene substrate. Furthermore, we provide crystallographic evidence of an organometallic aryl-Co(III) intermediate proposed in 8-aminoquinoline-directed Co-catalyzed C–H activation processes. Subsequent insights obtained from the application of our new organometallic aryl-Co(III) compounds in alkyne annulation reactions are also disclosed. Evidence obtained from the resulting regioselectivity of the annulation reactions and DFT studies indicates that a mechanism involving an organometallic aryl-Co(III)-alkynyl intermediate species is preferred for terminal alkynes, in contrast to the generally accepted migratory insertion pathway.



INTRODUCTION

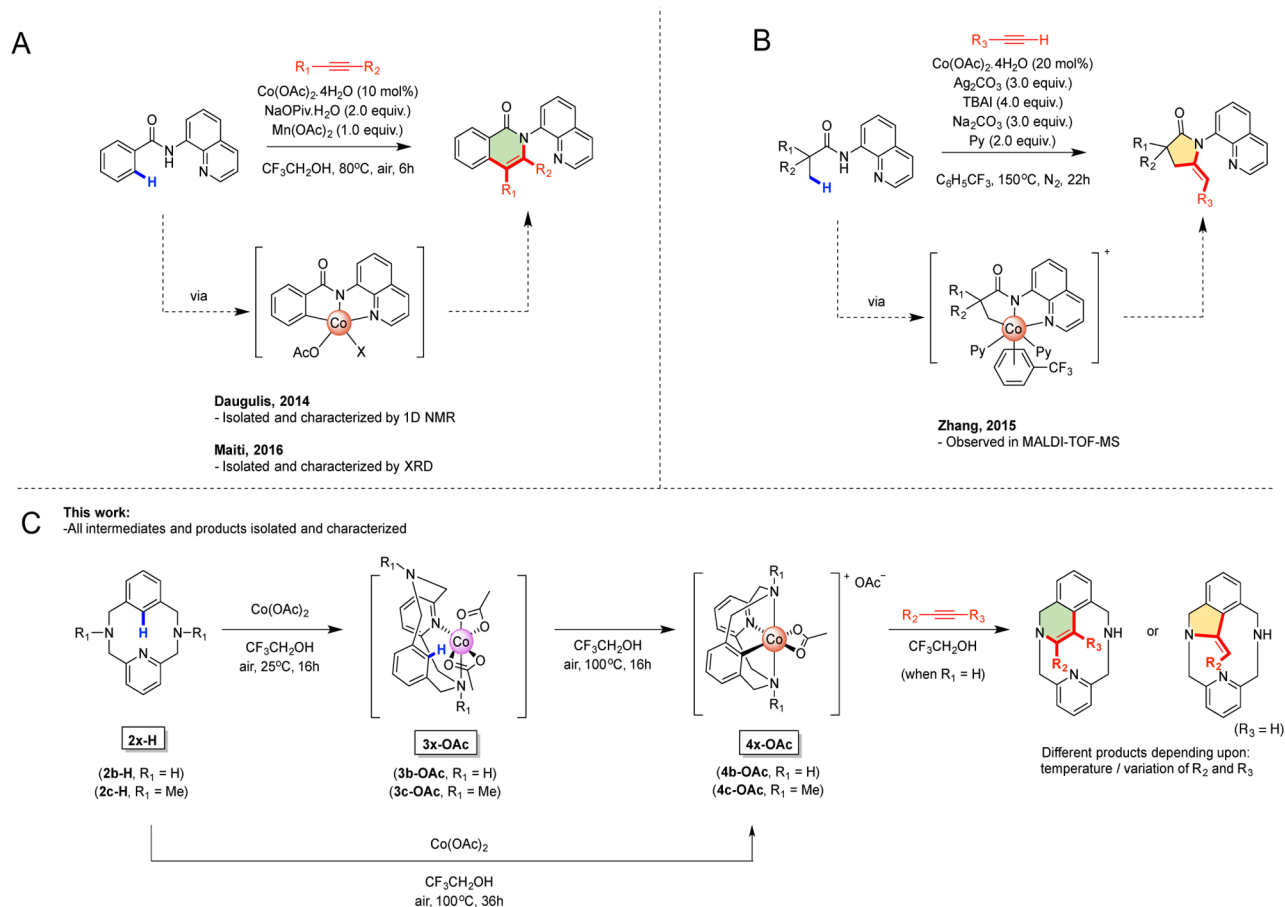
Selective functionalization of inert C–H bonds is currently attracting significant interest as the desire to develop new simplified protocols for the synthesis of complex pharmaceuticals, agrochemicals and natural products gathers pace.¹ Historically, most C–H activation and coupling protocols have been based on expensive, precious second- and third-row transition metals, most notably Pd.² More recently, the development of catalytic C–H functionalization protocols based on naturally more abundant and cheaper first-row transition metals, including Fe,³ Cu,⁴ Co,⁵ and Ni,⁶ has seen an explosion of activity. Unfortunately, mechanistic understanding concerning how these new first-row transition metal based protocols operate is significantly less advanced than their second- and third-row analogues. This is likely a consequence of the elusiveness and instability of key reaction intermediates, although there is an increasing interest in their detection and isolation.⁷ One reaction which is receiving particular interest at the current time is the annulation reaction of alkynes to substrates with inert C–H bonds, providing a facile route toward a variety of biologically and pharmaceutically relevant heterocyclic compounds. To date, Rh-catalysis has provided

significant success in this field,⁸ although the replacement of expensive Rh with a cheaper first-row transition metal has remained a challenge until recently. In this context, in 2013, Yoshikai reported the first synthesis of polysubstituted dihydropyridine derivatives, through a mild and facile cobalt-catalyzed alkyne annulation reaction.⁹ Since this report, an increasing number of Co-catalyzed annulation protocols have been reported using a range of coupling partners,¹⁰ including several examples highlighting the potential of alkynes.¹¹ Unfortunately, the mechanisms of these reactions are still relatively poorly understood, although organometallic Co(III) intermediates are generally implicated.⁵ Stable organometallic aryl-Co(III) compounds have been prepared via transmetalation reactions in the past,^{11g,12} although examples of the preparation of stable organometallic Co(III) compounds through direct C–H activation are still extremely rare, which has limited the understanding of this field. Organometallic aryl-Co(III) compounds derived from N-confused porphyrins and *m*-benzophthalocyanines have been metalated using Co(II) salts

Received: August 17, 2016

Published: October 10, 2016

Scheme 1. Characterized Organometallic Co(III) Intermediates in Co-Catalyzed Alkyne Annulation Protocols: (A) C(sp²)-H Activation and the Organometallic Aryl-Co(III) Intermediate Isolated by Daugulis and Co-workers and Maiti and Co-workers; (B) C(sp³)-H Activation and Organometallic Alkyl-Co(III) Intermediate Reported by Zhang and Co-Workers; (C) Overview of This Work, with Co(II) and Co(III) Intermediates and Annulation Products Characterized by 1D and 2D NMR, HRMS, XRD, and XAS



furnishing the Co(III) C-H activated products,¹³ although further reactivity studies were somewhat limited as a result of their stability.¹⁴

In the field of Co-catalyzed alkyne annulation protocols through C-H activation, the most solid experimental evidence so far of reaction intermediates has been provided by succinct NMR, MALDI-TOF, and most recently X-ray diffraction (XRD). In 2014, Daugulis and co-workers reported the preparation and characterization (1D NMR) of an organometallic aryl-Co(III) compound, obtained through C(sp²)-H activation, which was implicated as the key intermediate in a Co-catalyzed annulation protocol (Scheme 1A).^{11b} In 2015, Zhang and co-workers observed, by MALDI-TOF analysis of a crude reaction mixture during a Co(II)-catalyzed annulation reaction, evidence of an organometallic C(sp³)-Co(III) intermediate, resulting from direct activation of C(sp³)-H bonds (Scheme 1B).^{11a} Very recently, in a related study, Maiti and co-workers have successfully provided XRD evidence of a species invoked as an intermediate in Co-catalyzed alkene coupling reactions.¹⁵

Taking into account the increasing interest in Co-catalyzed transformations and the absence of benchtop-stable organometallic aryl-Co(III) compounds prepared through direct C-H activation, we became interested in the possibility of isolating organometallic aryl-Co(III) compounds, in order to understand

their synthesis, features and reactivity. Our approach was based on expertise within our laboratory using model macrocyclic arene substrates to successfully stabilize organometallic aryl-metal intermediate species, including Ni(II)¹⁶ and Cu(III).^{16,17} These isolable compounds have now been implicated as the intermediate species in a wide variety of cross-coupling transformations.

Herein, we will describe the synthesis and characterization of benchtop-stable organometallic aryl-Co(III) compounds obtained through C(sp²)-H activation, in a clear stepwise manner, using a 12-membered macrocyclic model substrate, which have been fully crystallographically and spectroscopically characterized. A similar macrocyclic substrate has previously been utilized to investigate the reactivity of organometallic Ni(III) intermediates.¹⁸ Subsequent insights obtained from the application of these isolable organometallic aryl-Co(III) intermediates in alkyne annulation reactions, in which they are proposed as key reaction intermediate (Scheme 1C) will also be disclosed, including evidence for an unprecedented “acetylide pathway” for terminal alkynes in annulation reactions. Putting this work into context, we also report crystallographic evidence of the sought-after organometallic aryl-Co(III) intermediate proposed in 8-aminoquinoline directed Co-catalyzed C-H activation processes.

RESULTS

Synthesis and Characterization of Organometallic Aryl-Co(III) Compounds. Macrocyclic model arene substrates **2b-H** and **2c-H** were synthesized through cyclization of the tosyl-protected amine **1** with 2,6-bis(bromoethyl)pyridine, followed by a deprotection of tosylated macrocyclic compound **2a-H**, furnishing **2b-H**, which could be further methylated at the secondary amines to obtain **2c-H** (see Scheme S1). Thereafter, Co(II) coordination compounds were prepared by reaction of Co(OAc)₂ with **2b-H** and **2c-H** (Scheme 1C), at 25 °C, using 2,2,2-trifluoroethanol (TFE) as solvent ([(**2b-H**)Co(II)(OAc)₂] (**3b-OAc**) and [(**2c-H**)Co(II)(OAc)₂] (**3c-OAc**)). The structure of **3b-OAc** was initially confirmed by HRMS ([M - OAc]⁺; calcd *m/z* = 357.0882; found 357.0874) and XRD analysis (see Figure S15). The solid-state molecular structure of **3b-OAc** indicated that the compound has two acetates coordinated in a bidentate fashion and that the potentially tridentate macrocycle acts as bidentate ligand (coordinated through only the pyridine and one amine). Upon performing the same reaction with CoBr₂ and **2c-H**, complex **3c-Br** was obtained, which in contrast, had both amines of the macrocyclic ligand coordinated (XRD, see Figure S16). Careful analysis of these crystal structures shows that the aryl C-H bond is out of plane (torsion angles of 14° for **3b-OAc** and 21° for **3c-Br**), indicating an incipient interaction between the Co(II) and hydrogen of the arene.

Upon reacting Co(OAc)₂ with **2b-H** and **2c-H** in TFE at 100 °C (or heating of the preformed **3b-OAc** and **3c-OAc**), complete conversion to the target organometallic aryl-Co(III) complexes, [(**2b**)Co(III)(η²-OAc)](OAc) (**4b-OAc**) and [(**2c**)Co(III)(η²-OAc)](OAc) (**4c-OAc**), was achieved (Scheme 1C). Due to the stability of the isolated organometallic aryl-Co(III) compounds, it was possible to characterize them by NMR and HRMS (Figure 1 and Figures S36–S45),

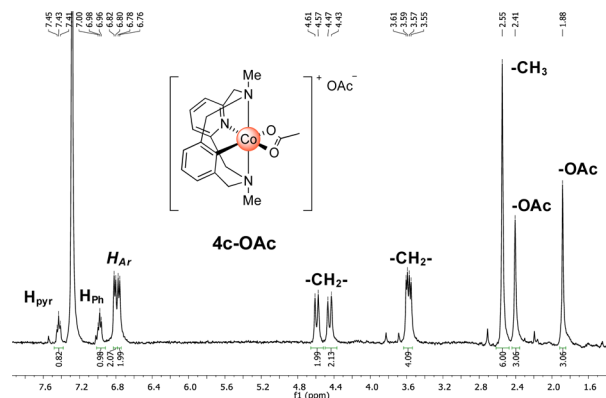


Figure 1. ¹H NMR spectrum with assignments for **4c-OAc** in CDCl₃ at 298 K.

providing spectra consistent with a low spin diamagnetic Co(III) metal center. Two nonequivalent acetate signals were observed, indicating that only one acetate is likely to be coordinated to the Co complex with the second acetate displaced as an outer-sphere counterion. The proposed structure was further supported by HRMS studies of **4b-OAc** and **4c-OAc**, which afforded clean spectra with major signals corresponding to the [(**2**)Co(III)(OAc)]⁺ ions (**4b-OAc**, [M - OAc]⁺; calcd *m/z* = 356.0804; found 356.0802; **4c-OAc**, [M - OAc]⁺; calcd *m/z* = 384.1117; found 384.1122). An analogous

organometallic Rh(III) complex (**5c-Cl**) was also prepared following a similar protocol (see Scheme S15 and Figure S17).

In our initial studies, XRD characterization of **4b-OAc** and **4c-OAc** remained elusive and as a result we turned to X-ray absorption spectroscopy (XAS) at the Co K-edge, in order to probe the electronic structure (XANES) and coordination environment (EXAFS) (Figure 2A–C and Figures S19–S22). Figure 2A shows the rising edge spectra for the starting material and the organometallic aryl-Co(III) **4b-OAc** and **4c-OAc** analogues. **3c-OAc** shows a weak pre-edge feature due to 1s →

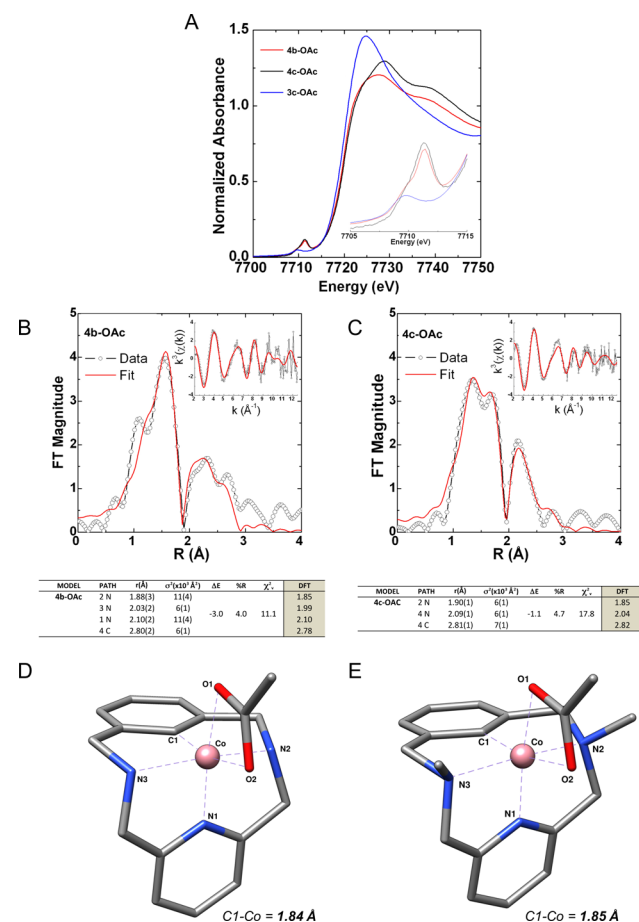
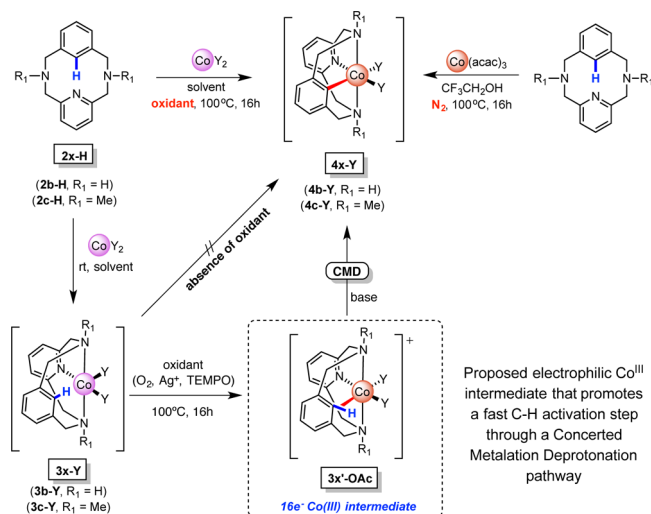


Figure 2. Characterization of aryl-Co(III) compounds through EXAFS spectroscopy. (A) XAS spectra at the Co K-edge highlighting the XANES region of the spectrum, and the 1s → 3d pre-edge transitions (inset). (B) EXAFS analysis of **4b-OAc**. Shown are Fourier-transformed EXAFS spectra (no phase correction, k-window = 2–12.5 Å⁻¹) as well as the k³-weighted unfiltered EXAFS spectra (inset) and comparison of selected EXAFS derived and theoretical bond distances (bottom table). (C) EXAFS analysis of **4c-OAc**. Shown are Fourier-transformed EXAFS spectra (no phase correction, k-window = 2–12.5 Å⁻¹) as well as the k³-weighted unfiltered EXAFS spectra (inset) and comparison of selected EXAFS derived and theoretical bond distances (bottom table). (D) Geometry optimized structure for **4b-OAc**. Selected bond distances [Å] and angles [°]: Co–C(1) 1.85, Co–N(1) 1.85, Co–N(2) 2.00, Co–N(3) 2.00, Co–O(1) 1.96, Co–O(2) 2.11; C(1)–Co–N(1) 89.8, C(1)–Co–N(2) 84.5, C(1)–Co–N(3) 84.4, C(1)–Co–O(1) 99.6, C(1)–Co–O(2) 164.9. (E) Geometry optimized structure for **4c-OAc**. Selected bond distances [Å] and angles [°]: Co–C(1) 1.85, Co–N(1) 1.85, Co–N(2) 2.05, Co–N(3) 2.05, Co–O(1) 1.96, Co–O(2) 2.11; C(1)–Co–N(1) 86.5, C(1)–Co–N(2) 84.6, C(1)–Co–N(3) 84.6, C(1)–Co–O(1) 101.0, C(1)–Co–O(2) 166.3.

3d transitions at ~ 7709.8 eV consistent with a Co(II) center having a centrosymmetric local environment.¹⁹ EXAFS analysis of **3c-OAc** shows a six coordinate complex with three pairs of Co–N/O scattering shells at 2.04, 2.22, and 2.35 Å, suggesting a distorted octahedral coordination environment at the metal center (Figure S20 and Table S15). XAS data for **3c-Br**, on the other hand, are consistent with the proposed 5-coordinate crystal structure (Figure S19 and Table S14). Upon C–H activation, a 0.5 eV shift in the rising edge at half height is observed for both **3c-OAc** and the **3b-OAc** analogue, concomitant with a ~ 1.6 eV shift to higher energy of the pre-edge, indicating oxidation of the metal center to Co(III).¹⁹ Additionally, the increase in intensity of the pre-edge feature observed, not only accounts for the increase in oxidation state and the extra electron hole, but also suggests a coordination geometry more favorable to p–d mixing. EXAFS analysis of **4b-OAc** and **4c-OAc** (Figure 2B,C) intermediates indicates the presence of two short N/O/C scattering atoms at ~ 1.89 Å and four longer N/O/C scattering paths with an average effective path length spanning ~ 2.04 – 2.09 Å. This is consistent with the proposed theoretical models that predict two short N/O/C pyridine nitrogen and C–H activated carbon (C_{phenyl}) and four longer scattering paths (~ 2.0 Å) coming from the tertiary amines and an acetate, resulting in a trigonal bipyramidal geometry at the metal center. The proposed structures for the **4b-OAc** and **4c-OAc** complexes are in agreement with the NMR and HRMS data (vide supra) and help to explain the intense pre-edge features from XAS, whereby a trigonal bipyramidal local metal geometry facilitates p–mixing into the d-manifold resulting in a more intense pre-edge.

Thereafter, formation of the organometallic aryl-Co(III) compounds was further studied (see Scheme 2 and Schemes S17–S19). It was found that the addition of 2.0 equiv of KOAc to a mixture of **2c-H** and CoBr_2 in MeCN resulted in complete conversion to **4c-OAc**, whereas in the absence of base a mixture of Co(II) complex **3c-Br** and Co(III) organometallic **4c-Br** was obtained, suggesting that both solvent and base have an important role in the C–H activation step. In particular,

Scheme 2. Formation of Aryl-Co(III) Intermediates: Optimization and Evaluation of Conditions Using Different Solvents (TFE, CH_3CN) and Oxidants (Air, Silver Salts, TEMPO) To Furnish Organometallic Aryl-Co(III) Intermediates through a C–H Activation Approach



fluorinated alcohols appear to be crucial (Table S2), as has previously been identified for a number of other metal-catalyzed transformations.²⁰ Preparation of the organometallic aryl-Co(III) compounds was also attempted under an inert atmosphere (N_2), but the reaction did not proceed when starting from Co(II) salts and **2c-H**. However, if the reaction was performed under an inert atmosphere in the presence of oxidants, such as silver salts or TEMPO, organometallic aryl-Co(III) intermediates could be detected using HRMS (Scheme S19 and Figures S5–S10). When $\text{Co}(\text{acac})_3$ was used as Co source, under an inert atmosphere, the corresponding organometallic aryl-Co(III) species (**4c-acac**) was formed as the major product (Figure S4). These observations indicate that Co(II) is likely first oxidized before the C–H activation step, forming a highly electrophilic penta-coordinated Co(III) $16e^-$ complex (Scheme 2, **3x'-OAc**). Interaction of Co(III) with the corresponding C–H bond promotes its deprotonation by the base (acetate, bromide or perchlorate in this study). These experimental observations lead us to propose that C–H bond cobaltation is likely to proceed via a concerted metalation–deprotonation (CMD) pathway.

As mentioned, it was not possible to obtain suitable crystals of **4x-OAc** for XRD studies. As reaction using silver salts as oxidant was also satisfactory, another strategy to grow crystals was followed; **3x-Br** was mixed with AgClO_4 (3.0 equiv) in an $\text{CH}_3\text{CN}/\text{TFE}$ (10:1) mixture at 100°C , whereby the corresponding organometallic complex **4x- CH_3CN** was obtained (see Schemes S13 and S14 and Figures S13 and S14). Crystals of **4b- CH_3CN** , as well as **4c- CH_3CN** , suitable for XRD studies were this time obtained and fully characterized using XRD and other techniques (Figure 3A,B and Figures S46–S55). The experimentally determined EXAFS Co– C_{phenyl} bond distances of 1.88 Å for **4b-OAc** and 1.90 Å for **4c-OAc** (Figure 2B–E) are consistent with the Co(III)– C_{phenyl} distance of 1.86

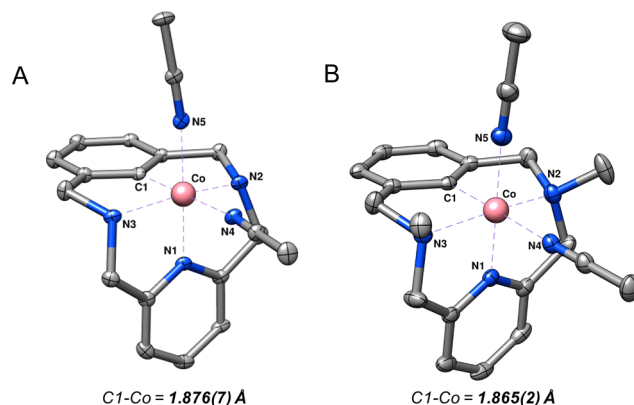


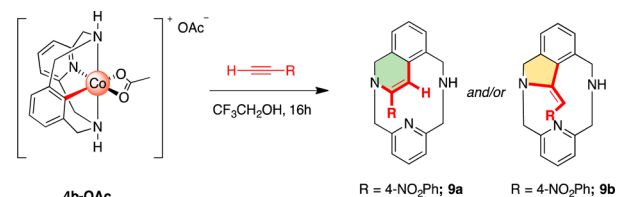
Figure 3. Solid-state structures of organometallic aryl-Co(III) compounds. Hydrogen atoms, perchlorate anions and solvent molecules have been omitted for clarity; ellipsoids are set at 50% probability. (A) Crystal data for **4b- CH_3CN** . Selected bond distances [Å] and angles [°]: Co–C(1) 1.876(7), Co–N(1) 1.853(4), Co–N(2) 1.997(6), Co–N(3) 2.008(5), Co–N(4) 2.025(6), Co–N(5) 1.897(4); C(1)–Co–N(1) 90.55(2), C(1)–Co–N(2) 83.68(2), C(1)–Co–N(3) 83.66(2), C(1)–Co–N(4) 177.87(2), C(1)–Co–N(5) 88.40(2). (B) Crystal data for **4c- CH_3CN** . Selected bond distances [Å] and angles [°]: Co–C(1) 1.865(2), Co–N(1) 1.856(2), Co–N(2) 2.029(2), Co–N(3) 2.027(2), Co–N(4) 1.999(2), Co–N(5) 1.927(2); C(1)–Co–N(1) 88.16(9), C(1)–Co–N(2) 84.13(9), C(1)–Co–N(3) 84.26(9), C(1)–Co–N(4) 178.30(9), C(1)–Co–N(5) 91.30(9).

Å determined for both **4b-CH₃CN** and **4c-CH₃CN** from their crystal structures (Figure 3A,B). In order to put our new organometallic aryl-Co(III) compounds into context, we have also been able to obtain XRD evidence of an aryl-Co(III) intermediate furnished through assistance of the 8-aminoquinoline directing group.²¹ Using a nitro-derivative of the aminoquinoline scaffold (**6**),²² together with the addition of 2,2'-bipyridine (bipy), we were able to successfully crystallize this sought-after intermediate, [(**6**)Co(III)(bipy)(OAc)] (**8**) (Scheme S16 and Figure S18). This result sets definitive proof of the structure of this intermediate organometallic species and highlights the relevance of our new isolable organometallic aryl-Co(III) compounds for studying high-valent Co-catalyzed C(sp²)-H annulation reactions.

Study of Isolated Organometallic Aryl-Co(III) Compounds in Stoichiometric Alkyne Annulation Reactions.

With the isolated organometallic aryl-Co(III) compounds in hand, we then turned our attention toward the reactivity of **4b-OAc** using alkynes as coupling partners to furnish annulated products. We envisioned that this compound may provide similar products to the previously reported Co-catalyzed annulation reactions with alkynes,¹¹ which are believed to proceed via β -migratory insertion of the alkyne into the organometallic aryl-Co(III) bond, furnishing a dihydroisoquinoline product (6-membered ring, **9a** and **10a**) upon reductive elimination of the Co with our macrocyclic ligand. However, reaction of **4b-OAc** with 1-ethynyl-4-nitrobenzene at 100 °C in TFE unexpectedly resulted in the regioselective formation of the dihydroisoindoline product **9b** (5-membered ring) in good yields (Table 1, entry 1). The unexpected formation of **9b** led

Table 1. Reactivity of Organometallic Aryl-Co(III) Complex **4b-OAc with Terminal Alkynes as Coupling Partners**



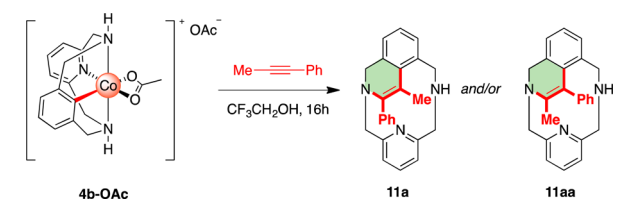
entry ^a	R	atm	temp (°C)	yield ^b (%)	ratio (a:b) ^c
1	4-NO ₂ Ph	air	100	54	1:99 (9a:9b)
2	4-NO ₂ Ph	air	60	66	1:12
3	4-NO ₂ Ph	air	rt	63	1:1.5
4	4-NO ₂ Ph	N ₂	60	60	1:12
5	Ph	air	100	30	99:1 (10a:10b)
6	Ph	air	60	36	99:1
7	Ph	air	rt	40	4:1
8	Ph	N ₂	60	34	99:1

^aReaction conditions: **4b-OAc** (40 mg, 0.077 mmol) and alkyne (2.0 equiv) were mixed in TFE and stirred at different temperatures and atmospheres over 16 h. ^bProducts were isolated using silica-gel chromatography. ^cRatios were determined by NMR spectrometry.

us to explore this reactivity further, changing the reaction conditions, such as temperature and electronic properties of the alkyne coupling partner. Thus, reactions with 1-ethynyl-4-nitrobenzene were carried out at lower temperatures (Table 1, entries 2 and 3) and interestingly, mixtures of **9a** and **9b** were obtained, with increasing ratio of **9a** with decreasing temperature.

This result suggests that **9b** is the thermodynamic product, while **9a** is the kinetic product. The structure of **9a** and **9b** were unambiguously determined using NMR and MS techniques (see Supporting Information for more details). Interestingly, under an inert atmosphere it was also possible to obtain products (Table 1, entry 4), indicating that no oxidant is required in the annulation reaction. Thereafter, reaction of **4b-OAc** with phenylacetylene was tested at 100 °C in TFE, which resulted in the selective formation of the 6-membered ring product **10a** (Table 1, entry 5). Surprisingly, other 6-membered ring isomers were never observed, showing that the reaction is regioselective toward the dihydroisoquinoline product **10a**. The same results were obtained when reactions were carried out at 60 °C in TFE, under air or N₂ atmospheres. However, when reactions were carried out at room temperature, a mixture of **10a** and **10b** was obtained (Table 1, entries 6 and 7). Therefore, contrary to the reaction with 1-ethynyl-4-nitrobenzene, for the reaction with phenylacetylene the thermodynamic product is **10a**, while **10b** is the kinetic product. Finally, the reactivity of the aryl-Co(III) compounds with an internal alkyne, 1-phenyl-1-propyne, was also evaluated. At 100 °C in TFE the reaction furnished 1,2-dihydroisoquinoline product (**11a**) in good yield (Table 2, entry 1). Variation of temperature resulted in the formation of both regioisomers, **11a** and **11aa** (Table 2, entries 2 and 3), suggesting again kinetic and thermodynamic products.

Table 2. Reactivity of Organometallic Aryl-Co(III) Complex **4b-OAc with 1-Phenyl-1-propyne as Coupling Partner**

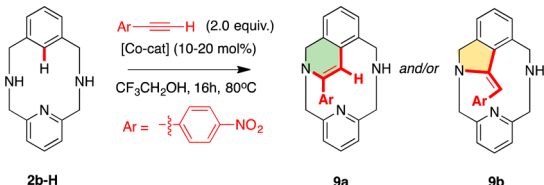


entry ^a	atm	temp (°C)	yield ^b (%)	Ratio ^c (11a:11aa)
1	air	100	72	99:1
2	air	60	70	4:1
3	air	rt	54	2:1
4	N ₂	60	65	4:1

^aReaction conditions: **4b-OAc** (0.077 mmol) and 1-phenyl-1-propyne (1.0 equiv) were mixed in TFE and stirred at different temperatures and atmospheres over 16 h. ^bProducts were isolated using silica-gel chromatography. ^cRatios were determined by ¹H NMR.

Study of Isolated Aryl-Co(III) Compounds in Catalytic Alkyne Annulation Reactions.

The annulation reaction was also studied in a catalytic fashion using **2b-H** and terminal alkynes. Initial tests were performed using catalytic quantities of Co(OAc)₂, **3b-OAc** and **4b-OAc**, together with 1-ethynyl-4-nitrobenzene and **2b-H** (Table 3). At room temperature, starting from Co(OAc)₂ the reactions did not proceed, in contrast to the stoichiometric experiments described above (Table 1, entries 3 and 7). This result indicates that C-H activation is the rate-determining step for these transformations, in agreement with what is suggested for most studies in this field. 1-ethynyl-4-nitrobenzene was successfully coupled to **2b-H** at 80 °C using TFE as solvent, under an oxygenated atmosphere, with 20 mol% of Co(OAc)₂, **3b-OAc** or **4b-OAc** (Table 3, entries 1, 3, and 7).

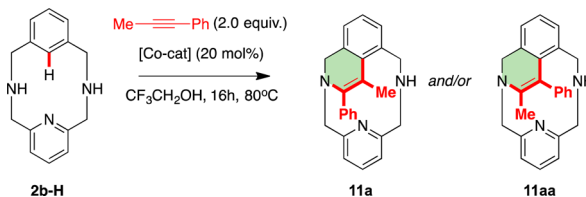
Table 3. Study of off-Cycle Intermediates in Catalytic Reactions Starting from 2b-H and Terminal Alkynes


entry ^a	[Co] (x mol%)	atm	yield ^b (%)	ratio ^c (9a:9b)
1	Co(OAc) ₂ (20)	air	66	1:99
2	Co(OAc) ₂ (20)	N ₂	5 ^d	n.d.
3	4b-OAc (20)	air	69	1:99
4	4b-OAc (20)	N ₂	13 ^d	1:99
5	4b-OAc (10)	air	43	1:99
6	4b-OAc (10)	N ₂	trace ^d	n.d.
7	3b-OAc (20)	air	58	1:99
8	3b-OAc (20)	N ₂	7 ^d	n.d.

^aReaction conditions: 2b-H (0.077 mmol) and 1-phenyl-1-propyne (2.0 equiv) were mixed in TFE with 10–20 mol% of 4b-OAc and stirred at 100 °C under different atmospheres over 16 h. ^bProducts were isolated using silica-gel chromatography. ^cRatios were determined by ¹H NMR. ^dYield determined using 1,3,5-trimethoxybenzene as internal standard.

Under an inert atmosphere the reaction was significantly retarded when starting from both Co(II) precursors or the off-cycle intermediate 4b-OAc (Table 3, entries 2, 4 and 8), suggesting that an external oxidant is needed to regenerate the catalyst.

Next, the annulation reaction with internal alkynes was tested in a catalytic fashion. At 80 °C, 1-phenyl-1-propyne could be coupled to 2b-H in good yields under air using 20 mol% of Co(OAc)₂ or the proposed off-cycle intermediates 3b-OAc and 4b-OAc, obtaining similar yields and regioselectivities (Table 4, entries 1, 3, and 5). As with the terminal alkynes, under an inert

Table 4. Study of off-Cycle Intermediates in Catalytic Reactions Starting from 2b-H and 1-Phenyl-1-propyne


entry ^a	[Co] (20 mol%)	atm	yield ^b (%)	ratio ^c (11a:11aa)
1	Co(OAc) ₂	air	67	5:1
2	Co(OAc) ₂	N ₂	trace ^d	n.d.
3	4b-OAc	air	64	5:1
4	4b-OAc	N ₂	14 ^d	5:1
5	3b-OAc	air	66	5:1
6	3b-OAc	N ₂	trace ^d	n.d.

^aReaction conditions: 2b-H (0.077 mmol) and internal alkyne (2.0 equiv) were mixed in TFE with 20 mol% of 4b-OAc and stirred at 100 °C under different atmospheres over 16 h. ^bProducts were isolated using silica-gel chromatography. ^cRatios were determined by ¹H NMR. ^dYield determined using 1,3,5-trimethoxybenzene as internal standard.

atmosphere the reaction did not proceed starting from 3b-OAc or Co(OAc)₂ (Table 4, entries 2 and 6) and a 14% yield was obtained starting from 4b-OAc (Table 4, entry 4), highlighting the necessity for air to regenerate the required +3 oxidation state of Co for catalytic turnover.

Mechanistic Insights. From the experimental studies we can conclude that initially Co(OAc)₂ coordinates to 2b-H to furnish 3b-OAc. The new ligand environment permits facile oxidation to Co(III) followed by C–H cobaltation, which we propose proceeds through a concerted metalation deprotonation (CMD) process, furnishing 4b-OAc. Starting from the key aryl-Co(III) intermediates, BP86/B3LYP calculations (Figures 4–6) revealed that reaction with terminal alkynes proceeds following detachment of the η²-OAc resulting in a mono-coordinated acetate (A, ΔG = 18.5 kcal mol⁻¹), followed by a formation of an adduct with the incoming terminal alkyne with the metal complex (B, ΔG = 20.6 kcal mol⁻¹) and finally coordination of the alkyne to furnish a cationic π-complex (Figure 4, 4b-alkyne-OAc, ΔG = 19.1 kcal mol⁻¹). At this point

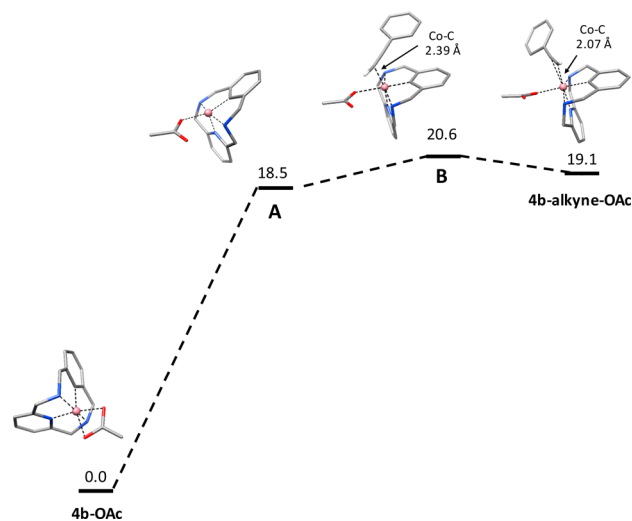
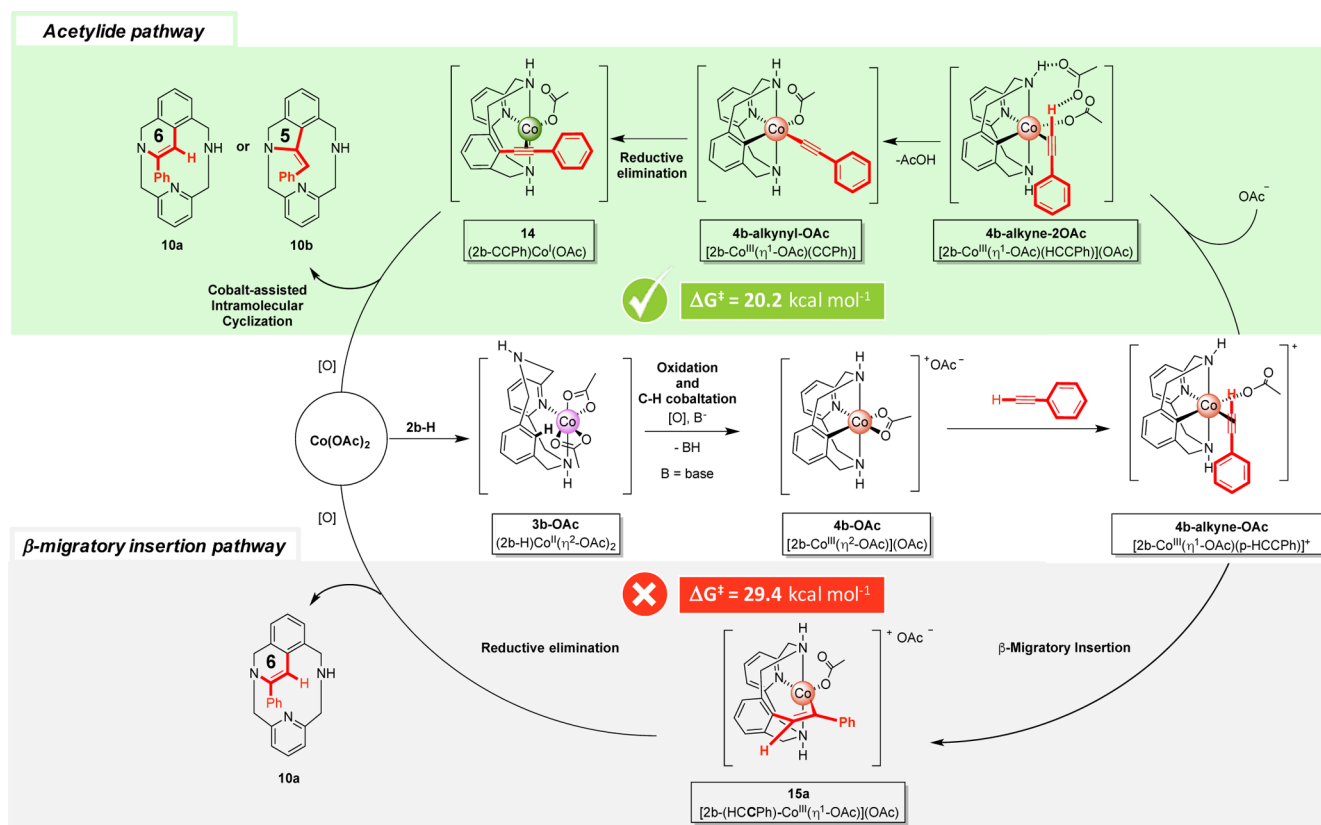


Figure 4. Gibbs energy profile of the formation of 4b-alkyne-OAc. Relative Gibbs energy values are given in kcal mol⁻¹ and selected bond distances in Å. Hydrogens not involved in reactivity are omitted for clarity (N, blue; O, red; Co(III), orange; C, gray; H, white).

the mechanism can diverge to two different pathways, i.e., the “acetylide pathway” (Scheme 3, upper green highlighted route) and the “migratory insertion pathway” (Scheme 3, lower gray highlighted route). In order to fully understand the implication of our experimental results, DFT studies were applied to distinguish whether the 6-membered ring products 9a and 10a were formed via the “acetylide pathway” or the prototypical β-migratory insertion when using phenylacetylene as alkyne coupling partner.

In the “acetylide pathway” (Figure 5), acetate-assisted deprotonation of the alkyne occurs via 4b-alkyne-2OAc (ΔG = 17.5 kcal mol⁻¹), which presents a hydrogen bond between the alkyne and one acetate anion. Subsequent proton transfer from the alkyne to the acetate anion and loss of acetic acid results in a low spin Co(III) acetylide intermediate, 4b-alkynyl-OAc (ΔG = 3.7 kcal/mol), through a 20.2 kcal mol⁻¹ transition state. Then, reductive elimination from 4b-alkynyl-OAc produces [(2b-CCPh)Co^I](OAc) (14), which is computed to be most stable as a triplet state by 19.3 kcal mol⁻¹. The most accessible C–C coupling pathway then proceeds from the

Scheme 3. Proposed Mechanistic Cycle of Co-Catalyzed Phenylacetylene Annulation through Aryl-Co(III) Intermediates Starting from $\text{Co}(\text{OAc})_2$ and Macrocyclic Ligand 2b-H^a 

^aThe highest energy barrier for each pathway indicated. Color code for Co oxidation state: green, (I); pink, (II); and orange, (III).

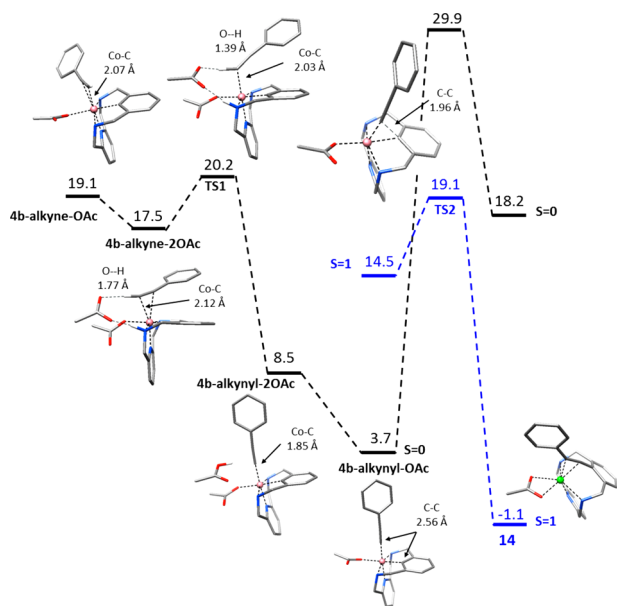


Figure 5. Gibbs energy profile of the formation of the acetylide pathway. Relative Gibbs energy values are given in kcal mol^{-1} and selected bond distances in Å. Hydrogens not involved in reactivity are omitted for clarity (N, blue; O, red; Co, pink; Co(III), orange; Co(I), green; C, gray; H, white).

singlet form of **4b-alkynyl-OAc**, which after a spin-crossing to the $S = 1$ state overcomes an overall barrier of $19.1 \text{ kcal mol}^{-1}$. Thereafter, a Co-assisted intramolecular cyclization furnishes

either the dihydroisoquinoline (6-membered ring, **10a**) or dihydroisoindoline (5-membered ring, **10b**) product depending on both the reaction temperature and the electronic properties of the alkyne.

In the “ β -migratory insertion pathway” (Figure 6), no deprotonation occurs and **4b-alkyne-OAc** undergoes β -migratory insertion toward the commonly proposed 7-membered cyclic intermediate (**15a**, Scheme 3), with a barrier of ($\Delta G^\ddagger = 29.4 \text{ kcal mol}^{-1}$). Thereafter, reductive elimination from **15a** furnishes the 6-membered ring **10a**, whereas the 5-membered product **10b** cannot be obtained through this mechanism.

Our experimental observations of the formation of **10a** and **10b** when **4b-OAc** is reacted with phenylacetylene and the higher energy barrier to form **15a** ($\Delta\Delta G^\ddagger = 9.2 \text{ kcal mol}^{-1}$) indicate that the key intermediate is likely to be an organometallic aryl-Co(III)-alkynyl species (**4b-alkynyl-OAc**, Figure 5 and Scheme 2). Thus, our proposal involves the deprotonation of the terminal acetylene by an acetate anion and the subsequent formation of an organometallic aryl-Co(III)-alkynyl intermediate, **4b-alkynyl-OAc**, which furnishes the linear intermediate **14** after a reductive elimination (upper green highlighted route in Scheme 3). Then, it is proposed that 6-membered ring (**9a** and **10a**) or 5-membered ring (**9b** and **10b**) products are obtained through a nucleophilic attack of one of the lateral amines through a Co-assisted intramolecular cyclization. Taking into account the DFT calculations, we propose that the mechanism exclusively operates through an “acetylide pathway”, whereas the commonly proposed “migratory insertion pathway” is excluded for terminal alkynes.

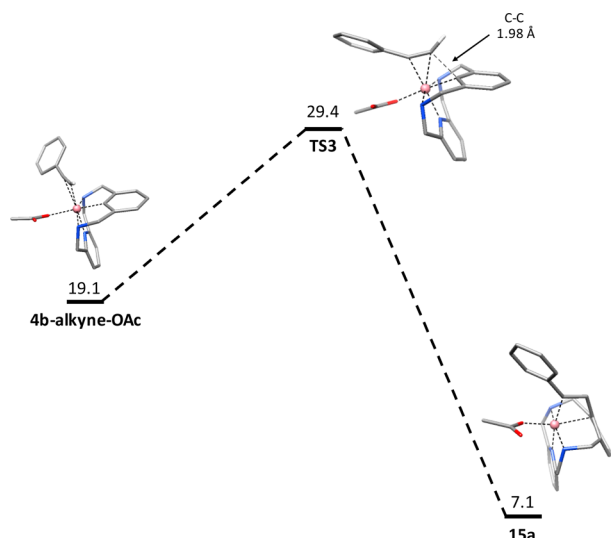


Figure 6. Gibbs energy profile of the formation of the β -migratory insertion pathway. Relative Gibbs energy values are given in kcal mol⁻¹ and selected bond distances in Å. Hydrogens not involved in reactivity are omitted for clarity (N, blue; O, red; Co(III), orange; C, gray; H, white).

Furthermore, the fact that no other 6-membered ring regioisomers are detected under any experimental conditions further supports the “acetylide pathway” operating for terminal acetylenes.

Our proposed mechanism also provides potential reasoning for experimental observations reported by Song,^{11f,k} Glorius,^{11h} and Ackermann^{11j} for other Co(III)-catalyzed annulation protocols displaying different selectivity, but starting from identical substrates. Furthermore, formation of **4b-alkynyl-OAc** is consistent with both the previously described organometallic Co(III) acetylide complexes²³ and the organometallic aryl-Co(III)-alkynyl species proposed by Zhang,^{11a} Song,^{11f,k} and Balaraman²⁴ in alkyne annulation reactions. Additionally, formation of two regioisomers (**10a** and **10b**) from a common starting material (**14**, Scheme 3, upper green highlighted route) can be explained by a nucleophilic attack of a lateral amine to one of the C(sp) centers. The kinetically and thermodynamically favored products depend on the substituents attached to the phenyl group.²⁵ On the other hand, when using internal alkynes (e.g., 1-phenyl-1-propyne) the organometallic aryl-Co(III)-alkynyl intermediate species are not accessible. However, DFT calculations show that the migratory insertion pathway is a plausible mechanism (see Figure S23). Therefore, we propose formation of **11a** and **11aa** via the β -migratory insertion and reductive elimination from a 7-membered ring intermediate analogous to **15a**. Recently, Zhang and co-workers have provided MALDI-TOF evidence of the formation of these intermediates.²⁶

CONCLUSIONS

In summary, we have prepared a number of organometallic aryl-Co(III) complexes using model macrocyclic arene substrates which enable the isolation and complete spectroscopic characterization of these key intermediates in Co-catalyzed C–H activation protocols. The design of the model arene substrates **2b-H** and **2c-H** is key for the stabilization of the organometallic aryl-Co(III) in a preferred-octahedral environment. Additionally, we provide definitive crystallo-

graphic proof of a sought-after organometallic aryl-Co(III) intermediate proposed in 8-aminoquinoline directed Co-catalyzed C–H activation processes. Reaction of organometallic aryl-Co(III) intermediates has been proven to follow different reaction pathways depending on the nature of the alkyne coupling partners. Terminal alkynes furnished 5- and 6-membered ring products depending on both the electronic properties of the alkynes and the reaction temperature. Clear evidence arising from the regioselectivity of the annulation reactions, in combination with a DFT study, indicates that the “acetylide pathway” is preferred for terminal alkynes, in contrast to the usually proposed “ β -migratory insertion pathway”. These findings strongly suggest that the “acetylide pathway” is general for terminal alkynes, representing the first solid experimental evidence of an organometallic aryl-Co(III)-alkynyl intermediate in alkyne C–H annulation reactions. This work constitutes a unique fundamental basis for the understanding of Co-catalyzed C–H activation protocols.

METHODS

XAS Data Acquisition and processing. Samples were prepared as solids diluted in boron nitride, loaded into holders with Kapton windows and stored at liquid nitrogen temperatures until run. All data was collected in transmission mode. Complexes **3c-Br** and **3c-OAc** were run under vacuum at 77 K using a liquid nitrogen finger dewar available from the XAFS beamline at Elettra Sincrotrone Trieste (2.0 GeV, 300 mA storage ring) equipped with a Si(111) double crystal monochromator. Data on the **4c-OAc** complex were collected at 77 K using a liquid nitrogen cryostat and a Si(111) double-crystal monochromator available at Diamond Light Source (3.0 GeV, 300 mA storage ring) beamline B18. Lastly data on the **4b-OAc** species was collected at SOLEIL synchrotron (2.75 GeV, 400 mA storage ring) at 20 K using a liquid helium cryostat and Si(220) double crystal monochromator. Data calibration and normalization were carried out using the Athena software package. Energies were calibrated to the first inflection point of Co foil spectra set at 7709.5 eV. A linear pre-edge function and a quadratic polynomial for the postedge were used for background subtraction and normalization of the edge jump. EXAFS data was extracted using the AUTOBK algorithm with a spline between $k = 1$ and 15 \AA^{-1} having a R_{bkg} value of 1.0 Å. EXAFS analysis was carried out with the Artemis software program running the IFEFFIT engine and the FEFF6 code.²⁷ Unless otherwise specified k^3 -weighted data was fit in r -space using a Hannings window ($dk = 2$) over a k -range of $2\text{--}12.5 \text{ \AA}^{-1}$, and an r -range of $1\text{--}3 \text{ \AA}$. The S_0^2 value was set to 0.9, and a global ΔE_0 was employed with the initial E_0 value set to the inflection point of the rising edge. Single and multiple scattering paths were fit in terms of a Δr_{eff} and σ^2 as previously described.²⁸ To assess the goodness of the fits the R_{factor} (%R) was minimized. Overfitting the data was controlled by minimizing the number of adjustable parameters and ensuring that the reduced χ^2 (χ^2_{v}) decreases with increasing number of adjustable parameters.

Density Functional Theoretical Calculations. Theoretical calculations were carried out using the ORCA package.²⁹ Geometry optimizations were carried out using the spin-unrestricted Kohn–Sham formalism employing a BP86 functional³⁰ with a def2-TZVP(-f) basis set on the metal, nitrogens and oxygens, a SVP basis set on the hydrogens and def2-SVP on carbons, as well as a def2-TZVP/J auxiliary basis set on all atoms.³¹ A dense integration grid (ORCA Grid 5 = Lebedev 434 points) was used for all atoms. Furthermore, dispersion corrections were included using the Grimme and co-workers DFT-D3BJ approach³² and solvent effects were incorporated using a conductor like screening model (COSMO) using 2,2,2-trifluoroethanol as solvent ($\epsilon = 27$). Subsequent frequency calculations were done to evaluate enthalpy and entropy corrections at 298.15 K (G_{corr}) and ensured that all local minima had only real frequencies while a single imaginary frequency confirmed the presence of transition states. Single-point calculations on the equilibrium geo-

metries, including the solvent effects and D3BJ dispersion corrections were computed using the B3LYP functional and def2-TZVPP basis set for all the atoms (E_{B3LYP}). The density fitting and chain of spheres (RIJCOSX) approximations³³ were employed together with the def2-QZVP/JK auxiliary basis set.³¹ The free energy change associated with moving from a standard-state gas phase pressure of 1 atm to a standard state gas phase concentration of 0.046 M for solutes ($\Delta G^{\circ/*}$) was also included in the final free energies. The value of $\Delta G^{\circ/*}$ at 298.15 K is 0.079 kcal mol⁻¹ for 0.046 M standard state solutes. Then, the final total Gibbs free energy (G) was given by

$$G = E_{\text{B3LYP}} + G_{\text{corr}} + \Delta G^{\circ/*} \quad (1)$$

Representative C–H Cobaltation of 2b-H and 2c-H. In a 10 mL vial, 2b-H or 2c-H (0.41 mmol) and Co(OAc)₂ (0.41 mmol) were mixed in TFE (2.5 mL). The vial was then sealed with a septum, and the mixture was heated at 100 °C for 36 h. Thereafter, the solvent was removed, and the crude was dissolved in CHCl₃ and layered with pentane. After 24 h at 4 °C, the resulting oil was dried under vacuum for 6 h, giving the product as a gray-red foam (58–70%).

Representative Stoichiometric Reaction of 4b-OAc with Alkynes. In a 2 mL vial, 4b-OAc (40 mg, 0.077 mmol) and alkyne (0.077 mmol) were mixed in TFE (1.5 mL). The vial was then sealed with a septum, and the mixture was stirred for 16 h at different temperatures. After removal of TFE, NH₄OH (2 mL) was added, and the solution was extracted using CH₂Cl₂ (2 × 5 mL). Products were purified by column chromatography on silica gel (CH₂Cl₂ then CH₂Cl₂/MeOH 95:5) and characterized by NMR techniques and HRMS (see Supporting Information for full details).

Representative Catalytic Reaction of 4b-OAc with Alkynes. In a 2 mL vial, 2b-H (0.077 mmol) and alkyne (0.154 mmol) were mixed in TFE (1.5 mL) with 10–20 mol% of 4b-OAc. The vial was then sealed with a septum, and the mixture was stirred for 16 h at 80 °C. After removal of the solvent, NH₄OH (2 mL) was added, and the solution was extracted using CH₂Cl₂ (2 × 5 mL). The products were then purified by column chromatography on silica gel (CH₂Cl₂, then CH₂Cl₂/MeOH 95:5) and characterized by NMR techniques. 1,3,5-Trimethoxybenzene was used as internal standard in selected cases (see Supporting Information for full details).

■ ASSOCIATED CONTENT

● Supporting Information

The Supporting Information is available free of charge on the ACS Publications website at DOI: 10.1021/jacs.6b08593.

General considerations, experimental details for the preparation and characterization of ligands 2b-H and 2c-H, and compounds 4b-OAc, 4c-OAc, 4b-CH₃CN, 4c-CH₃CN, 5c-Cl, 7 and 8; optimization details; experimental details of stoichiometric reactions of 4b-OAc with alkynes; experimental details of catalytic reactions of 4b-OAc with alkynes; XYZ coordinates for DFT structures; full XAS analysis; full characterization of compounds; X-ray parameters and original NMR spectra [including Schemes S1–S24, Tables S1–S41, and Figures S1–S85] (PDF)

X-ray crystallographic data for 3b-OAc (CIF)

X-ray crystallographic data for 3c-Br (CIF)

X-ray crystallographic data for 4b-CH₃CN (CIF)

X-ray crystallographic data for 4c-CH₃CN (CIF)

X-ray crystallographic data for 5c-Cl (CIF)

X-ray crystallographic data for 8 (CIF)

■ AUTHOR INFORMATION

Corresponding Author

*xavi.ribas@udg.edu

Notes

The authors declare no competing financial interest.

Crystallographic data for compounds 3b-OAc (CCDC-1493341), 3c-Br (CCDC-1493342), 4b-CH₃CN (CCDC-1493343), 4c-CH₃CN (CCDC-1493344), 5c-Cl (CCDC-1493345) and aryl-Co(III) species using nitro-aminoquinoline model substrate 8 (CCDC-1493346) can be obtained free of charge from the Cambridge Crystallographic Data Centre via www.ccdc.cam.ac.uk/data_request/cif.

■ ACKNOWLEDGMENTS

We acknowledge financial support from the European Research Council for the Starting Grant Project ERC-2011-StG-277801 to X.R. and from MINECO of Spain for project CTQ2013-43012-P to A.C. and X.R., CTQ2014-52525-P to J.M.L. and CTQ2015-64436-P to T.P. We also thank Generalitat de Catalunya for projects 2014SGR862 and 2014SGR931. We thank the MECED of Spain for a FPU PhD grant to O.P. and MINECO for a Ramón y Cajal contract to A.C. X.R. also thanks Generalitat de Catalunya for an ICREA-Acadèmia Award. In addition, the research leading to these results has received funding from the European Community's Seventh Framework Programme (FP7/2007-2013) under grant agreement no. 312284. XAS data was collected at Elettra and SOLEIL synchrotron facilities. We thank Dr. Luca Olivi from Elettra and Dr. Landrot Gautier from SOLEIL for their help with experimental setup. XRD (Xavi Fontrodona) and HRMS (Dr. Laura Gómez) data was collected at STR-UdG.

■ REFERENCES

- (1) Yamaguchi, J.; Yamaguchi, A. D.; Itami, K. *Angew. Chem., Int. Ed.* **2012**, *51*, 8960.
- (2) Chen, X.; Engle, K. M.; Wang, D.-H.; Yu, J.-Q. *Angew. Chem., Int. Ed.* **2009**, *48*, 5094.
- (3) (a) Bolm, C.; Legros, J.; Le Pailh, J.; Zani, L. *Chem. Rev.* **2004**, *104*, 6217. (b) Ambhaikar, N. *C-H Bond Activation in Organic Synthesis*; CRC Press: Boca Raton, FL, 2015; p 145.
- (4) (a) Guo, X.-X.; Gu, D.-W.; Wu, Z.; Zhang, W. *Chem. Rev.* **2015**, *115*, 1622. (b) Ahmad, N. *C-H Bond Activation in Organic Synthesis*; CRC Press: Boca Raton, FL, 2015; p 175.
- (5) (a) Moselage, M.; Li, J.; Ackermann, L. *ACS Catal.* **2016**, *6*, 498. (b) Wei, D.; Zhu, X.; Niu, J.-L.; Song, M.-P. *ChemCatChem* **2016**, *8*, 1242. (c) Gao, K.; Yoshikai, N. *Acc. Chem. Res.* **2014**, *47*, 1208.
- (6) (a) Tasker, S. Z.; Standley, E. A.; Jamison, T. F. *Nature* **2014**, *509*, 299. (b) Williams, A. *C-H Bond Activation in Organic Synthesis*; CRC Press: Boca Raton, FL, 2015; p 113.
- (7) Gensch, T.; Klauk, F. J. R.; Glorius, F. *Angew. Chem., Int. Ed.* **2016**, *55*, 11287.
- (8) (a) Colby, D. A.; Tsai, A. S.; Bergman, R. G.; Ellman, J. A. *Acc. Chem. Res.* **2012**, *45*, 814. (b) Song, G.; Wang, F.; Li, X. *Chem. Soc. Rev.* **2012**, *41*, 3651. (c) Satoh, T.; Miura, M. *Chem. - Eur. J.* **2010**, *16*, 11212.
- (9) Yamakawa, T.; Yoshikai, N. *Org. Lett.* **2013**, *15*, 196.
- (10) (a) Wu, X.; Yang, K.; Zhao, Y.; Sun, H.; Li, G.; Ge, H. *Nat. Commun.* **2015**, *6*, 6462. (b) Grigorjeva, L.; Daugulis, O. *Org. Lett.* **2014**, *16*, 4684. (c) Grigorjeva, L.; Daugulis, O. *Org. Lett.* **2014**, *16*, 4688. (d) Hummel, J. R.; Ellman, J. A. *J. Am. Chem. Soc.* **2015**, *137*, 490. (e) Zhao, D.; Kim, J. H.; Stegemann, L.; Strassert, C. A.; Glorius, F. *Angew. Chem., Int. Ed.* **2015**, *54*, 4508. (f) Gandeepan, P.; Rajamalli, P.; Cheng, C.-H. *Angew. Chem., Int. Ed.* **2016**, *55*, 4308. (g) Li, J.; Tang, M.; Zhang, L.; Zhang, X.; Zhang, Z.; Ackermann, L. *Org. Lett.* **2016**, *18*, 2742. (h) Li, L.; Wang, H.; Yu, S.; Yang, X.; Li, X. *Org. Lett.* **2016**, *18*, 3662. (i) Ma, W.; Ackermann, L. *ACS Catal.* **2015**, *5*, 2822. (j) Wang, H.; Lorion, M. M.; Ackermann, L. *Angew. Chem., Int. Ed.* **2016**, *55*, 10386.

- (11) (a) Zhang, J.; Chen, H.; Lin, C.; Liu, Z.; Wang, C.; Zhang, Y. *J. Am. Chem. Soc.* **2015**, *137*, 12990. (b) Grigorjeva, L.; Daugulis, O. *Angew. Chem., Int. Ed.* **2014**, *53*, 10209. (c) Nguyen, T. T.; Grigorjeva, L.; Daugulis, O. *ACS Catal.* **2016**, *6*, 551. (d) Planas, O.; Whiteoak, C. J.; Company, A.; Ribas, X. *Adv. Synth. Catal.* **2015**, *357*, 4003. (e) Kalsi, D.; Sundararaju, B. *Org. Lett.* **2015**, *17*, 6118. (f) Zhang, L.-B.; Hao, X.-Q.; Liu, Z.-J.; Zheng, X.-X.; Zhang, S.-K.; Niu, J.-L.; Song, M.-P. *Angew. Chem., Int. Ed.* **2015**, *54*, 10012. (g) Ikemoto, H.; Yoshino, T.; Sakata, K.; Matsunaga, S.; Kanai, M. *J. Am. Chem. Soc.* **2014**, *136*, 5424. (h) Lu, Q.; Vásquez-Céspedes, S.; Gensch, T.; Glorius, F. *ACS Catal.* **2016**, *6*, 2352. (i) Kim, J. H.; Greßies, S.; Glorius, F. *Angew. Chem., Int. Ed.* **2016**, *55*, 5577. (j) Mei, R.; Wang, H.; Warratz, S.; Macgregor, S. A.; Ackermann, L. *Chem. - Eur. J.* **2016**, *22*, 6759. (k) Hao, X.-Q.; Du, C.; Zhu, X.; Li, P.-X.; Zhang, J.-H.; Niu, J.-L.; Song, M.-P. *Org. Lett.* **2016**, *18*, 3610.
- (12) (a) Robitzer, M.; Bouamaïed, I.; Sirlin, C.; Chase, P. A.; van Koten, G.; Pfeffer, M. *Organometallics* **2005**, *24*, 1756. (b) Meneghetti, M. R.; Grellier, M.; Pfeffer, M.; Cian, A. D.; Fischer, J. *Eur. J. Inorg. Chem.* **2000**, *2000*, 1539.
- (13) (a) Harvey, J. D.; Ziegler, C. J. *Chem. Commun.* **2004**, *14*, 1666. (b) Çetin, A.; Sriphongnak, S.; Kawa, M.; Durfee, W. S.; Ziegler, C. J. *Chem. Commun.* **2007**, *41*, 4289.
- (14) Wang, Y.-C.; Chen, J.-H.; Wang, S.-S.; Tung, J.-Y. *Inorg. Chem.* **2013**, *52*, 10711.
- (15) Maity, S.; Kancherla, R.; Dhawa, U.; Hoque, E.; Pimparkar, S.; Maiti, D. *ACS Catal.* **2016**, *6*, 5493.
- (16) Ribas, X.; Calle, C.; Poater, A.; Casitas, A.; Gómez, L.; Xifra, R. I.; Parella, T.; Benet-Buchholz, J.; Schweiger, A.; Mitrikas, G.; Solà, M.; Llobet, A.; Stack, T. D. P. *J. Am. Chem. Soc.* **2010**, *132*, 12299.
- (17) (a) Casitas, A.; King, A. E.; Parella, T.; Costas, M.; Stahl, S. S.; Ribas, X. *Chem. Sci.* **2010**, *1*, 326. (b) Huffman, L. M.; Casitas, A.; Font, M.; Canta, M.; Costas, M.; Ribas, X.; Stahl, S. S. *Chem. - Eur. J.* **2011**, *17*, 10643. (c) King, A. E.; Huffman, L. M.; Casitas, A.; Costas, M.; Ribas, X.; Stahl, S. S. *J. Am. Chem. Soc.* **2010**, *132*, 12068.
- (18) (a) Zhou, W.; Schultz, J. W.; Rath, N. P.; Mirica, L. M. *J. Am. Chem. Soc.* **2015**, *137*, 7604. (b) Zhou, W.; Zheng, S.; Schultz, J. W.; Rath, N. P.; Mirica, L. M. *J. Am. Chem. Soc.* **2016**, *138*, 5777. (c) Zhou, W.; Rath, N. P.; Mirica, L. M. *Dalton Trans.* **2016**, *45*, 8693. (d) Zhou, W.; Watson, M. B.; Zheng, S.; Rath, N. P.; Mirica, L. M. *Dalton Trans.* **2016**, *45*, 15886.
- (19) Goswami, M.; Lyaskovskyy, V.; Domingos, S. R.; Buma, W. J.; Woutersen, S.; Troeppner, O.; Ivanović-Burmazović, I.; Lu, H.; Cui, X.; Zhang, X. P.; Reijerse, E. J.; DeBeer, S.; van Schooneveld, M. M.; Pfaff, F. F.; Ray, K.; de Bruin, B. *J. Am. Chem. Soc.* **2015**, *137*, 5468.
- (20) For examples of reactions where the use of fluorinated alcohols has proved highly beneficial, see: (a) Shuklov, I. A.; Dubrovina, N. V.; Börner, A. *Synthesis* **2007**, *2007*, 2925. (b) Wencel-Delord, J.; Colobert, F. *Org. Chem. Front.* **2016**, *3*, 394.
- (21) During the preparation of this manuscript, Maiti and co-workers reported a related XRD structure; see ref 15.
- (22) Whiteoak, C. J.; Planas, O.; Company, A.; Ribas, X. *Adv. Synth. Catal.* **2016**, *358*, 1679.
- (23) Cummins, D.; McKenzie, E. D.; Segnitz, A. *J. Organomet. Chem.* **1975**, *87*, C19.
- (24) Landge, V. G.; Jaiswal, G.; Balaraman, E. *Org. Lett.* **2016**, *18*, 812.
- (25) Rovira, M.; Font, M.; Acuña-Parés, F.; Parella, T.; Luis, J. M.; Lloret-Fillol, J.; Ribas, X. *Chem. - Eur. J.* **2014**, *20*, 10005.
- (26) Yu, W.; Zhang, W.; Liu, Z.; Zhang, Y. *Chem. Commun.* **2016**, *52*, 6837.
- (27) (a) Ravel, B.; Newville, M. *J. Synchrotron Radiat.* **2005**, *12*, 537. (b) Newville, M. *J. Synchrotron Radiat.* **2001**, *8*, 96. (c) Rehr, J. J.; Albers, R. C. *Rev. Mod. Phys.* **2000**, *72*, 621.
- (28) (a) Martin-Diaconescu, V.; Bellucci, M.; Musiani, F.; Ciurli, S.; Maroney, M. J. *JBIC, J. Biol. Inorg. Chem.* **2012**, *17*, 353. (b) Zambelli, B.; Berardi, A.; Martin-Diaconescu, V.; Mazzei, L.; Musiani, F.; Maroney, M. J.; Ciurli, S. *JBIC, J. Biol. Inorg. Chem.* **2014**, *19*, 319.
- (29) Becke, A. D. *Phys. Rev. A: At., Mol., Opt. Phys.* **1988**, *38*, 3098.
- (30) Neese, F. *Wiley Interdiscip. Rev. Comput. Mol. Sci.* **2012**, *2*, 73.
- (31) (a) Schäfer, A.; Horn, H.; Ahlrichs, R. *J. Chem. Phys.* **1992**, *97*, 2571. (b) Weigend, F.; Ahlrichs, R. *Phys. Chem. Chem. Phys.* **2005**, *7*, 3297.
- (32) (a) Grimme, S.; Antony, J.; Ehrlich, S.; Krieg, H. *J. Chem. Phys.* **2010**, *132*, 154104. (b) Grimme, S.; Ehrlich, S.; Goerigk, L. *J. Comput. Chem.* **2011**, *32*, 1456.
- (33) Neese, F.; Wennmohs, F.; Hansen, A.; Becker, U. *Chem. Phys.* **2009**, *356*, 98.